Materials Research 2019; 22(1): e20180530
DOI: http://dx.doi.org/10.1590/1980-5373-MR-2018-0530

Ag@Activated Carbon Felt Composite as Electrode for Supercapacitors and a Study of Three Different Aqueous Electrolytes

***Aline Castilho Rodrigues*[a,b,*], *Elen Leal da Silva*[b], *Sandro Fonseca Quirino*[c], *Andrés Cuña*[d], *Jossano Saldanha Marcuzzo*[b], *Jorge Tadao Matsushima*[e], *Emerson Sarmento Gonçalves*[a,f], *Mauricio Ribeiro Baldan*[a,b]**

[a]*Instituto Tecnológico da Aeronáutica, Praça Marechal Eduardo Gomes, 50, Vila das Acácias, CEP 12228-900, São José dos Campos, SP, Brasil*
[b]*Laboratório Associado de Materiais e Sensores, Instituto Nacional de Pesquisas Espaciais, Av. dos Astronautas, 1758, Jardim da Granja, CEP 12227-010, São José dos Campos, SP, Brasil*
[c]*ETEP Faculdades, Av. Barão do Rio Branco, 882, Jardim Esplanada, CEP 12242-800, São José dos Campos, SP, Brasil*
[d]*Cátedra de Fisicoquímica (DETEMA), Facultad de Química, Universidad de la República, General Flores, 11800, Montevideo, Uruguay*
[e]*Faculdade de Tecnologia Professor Jessen Vidal, Av. Cesare Mansueto Giulio Lattes, 1350, 12247-014, São José dos Campos, SP, Brasil*
[f]*Instituto de Aeronáutica e Espaço, Praça Marechal Eduardo Gomes, 50, Vila das Acacias, 12228-904, São José dos Campos, SP, Brasil*

Received: July 28, 2018; Revised: September 24, 2018; Accepted: October 08, 2018

The main challenge for the development of a high efficiency supercapacitor is the electrode material. Developing electrode materials with high specific electrical capacitance and low electrical resistance enables an increase in the energy accumulated in the device. In addition, it is expected that the electrode material presents a simple procedure for preparation having low production cost and being environmentally friendly. This work is based on the deposition of silver nanoparticles on activated carbon felt (Ag@ACF) as a supercapacitor electrode. The samples were characterized by field emission gun scanning electron microscopy, X-ray diffraction, X-ray photoelectron spectroscopy and textural analysis. Supercapacitor behavior was evaluated by galvanostatic charge-discharge curves, cyclic voltammetry and electrochemical impedance spectroscopy using a symmetrical two-electrode Swagelok type cell, and three different aqueous solution electrolytes: 2 M H_2SO_4, 6 M KOH and 1 M Na_2SO_4. Ag@ACF presented a high specific capacitance in KOH, about 170 F g^{-1}, which makes it an interesting material for supercapacitor electrodes and it showed good specific electrical capacitance, low resistance and high cyclability.

Keywords: *activated carbon felt, carbon-silver composite, energy storage, electrochemical properties, supercapacitor.*

1. Introduction

Nowadays, there is a great interest in renewable and clean energy sources due to energy demand related to the technological development as well as the preoccupation with the exhaustion of the natural resources. Based on these considerations, the development of electrochemical supercapacitors (ES), actually, is the focus of the technological research areas for energy demand regarding energy storage and conversion. ESs are known for their higher power density induced by a fast charging/discharging rate (in seconds) and a long cycle life (> 100000 cycles) when compared to batteries and fuel cells.[1,2] However, the major challenge has been to increase the storage capacity related to its energy density (W_S). Since the W_S of ESs depends on the capacitance (C) and square of the cell voltage (V), increasing either or both the C and V becomes an effective way to increase W_S. For this purpose, electrode materials with high capacitance, electrolytes with large working potential windows and integrated systems with a new and optimized structure have been explored.[3,4]

Referring to electrode materials, the activated carbon materials, with emphasis on activated carbon fibers (ACF) have been successfully explored due to their structural aspects associated with high specific area and high packing density as well as to their good electric conductivity.[5-12] In spite of these prominent aspects, ACF production with nano structures pore sizes with different textile forms can be explored.[4] However, there are not many studies of supercapacitor electrodes on activated carbon felt. Most of the studies involve activated

*e-mail: alinerodrigues_1@msn.com

carbons, commercial structural carbon fibers and other carbon materials.[7,11,13-16]

There are many studies about carbon material applied as supercapacitor electrodes relating the increase of energy and power density with the deposition of silver particles.[17-22] According to these studies, the presence of silver particles contributes to improve the electrical charge transfer, which results in an enhancement in the electrochemical performances of the composites. Kim and Park[23] studied the effect of the incorporation of silver nanoparticles on graphite nanofibers and PAni electrodes and found that silver considerably increases the specific capacitance, as well as increases the electrochemical utilization of the electrodes. Besides, the electrolyte type also influences the performance of ES due to the synergism promoted by the interaction between the ionic diffusion and the size of the electrolyte ions, which may increase the stored energy in association with the porous carbon structure. In particular, the electrolyte type has a major contribution to the energy density, because of its influence in the working potential window, i.e., enlarging V, which consequently, increases W_S.[24] There are many studies that study aqueous electrolytes. However, only a few compare the three electrolytes used in this work.[2-4]

Here we present preliminary studies on an unusual carbon fiber and we verify that it is possible to construct supercapacitor electrodes using carbon fibers of textile origin. The aim of this study is a comparison of different aqueous electrolytes in activated carbon felt (based on PAN-textile) composite electrode decorated with silver particles. Three electrolytes were investigated: 2 mol L^{-1} H_2SO_4, 1 mol L^{-1} Na_2SO_4 and 6 mol L^{-1} KOH, all widely used in the literature.

2. Experimental

The activated carbon fiber felt samples were prepared according to previews studies.[25] For the electrode sample preparation, an activated carbon felt (ACF) was immersed in a 2 g L^{-1} $AgNO_3$ aqueous solution up to saturating adsorption (24 hours). The sample was washed with deionized water and dried in a vacuum oven at 50ºC, forming an Ag@ACF composite.

The morphological analysis of the samples was performed through Field Emission Gun Scanning Electron Microscopy (FEG-SEM), model MIRA3 from TESAN. In order to obtain information regarding the crystal structure properties, the samples were analyzed by X-ray diffraction spectroscopy (XRD) using PANalytical series X'PertPRO diffractometer.

X-ray photoelectron spectroscopy (XPS) measurements were carried out with a Kratos Axis Ultra XPS spectrometer using a monochromated Al-Kalpha (1486.5 eV) X-ray radiation at 15kV ~ 150W. The emitted photoelectrons were detected using a hemispherical analyzer and a 15 µm spatial resolution. The vacuum system was maintained at approximately 10^{-9} Torr during all the experiments. Survey scans were collected from 0 to 1100 eV with pass energy equal to 160 eV with step size of 1 eV, in order to identify elements present on the surface, and pass energy of 40 eV for high resolution scans on specific atomic peaks.

Textural parameters were obtained from N_2 adsorption-desorption isotherms at 77 K using a Beckman Coulter SA 3100 apparatus. Before the experiments, degasification of samples was performed at 200ºC and 10^{-2} Pa for 20 h. The analysis by BET and NLDFT was used to determine the surface area and porosity data.[26]

For the electrochemical analysis, two-electrode Swagelok®-type cells having two tantalum rods as current collectors were used for galvanostatic charge/discharge, cyclic voltammetries and electrochemical impedance spectroscopy (EIS) measurements. Glassy microfiber paper (Whatman 934 AH) was used as a separator between the two electrodes. Ag@ACF, with a cross-section area of 0.8 cm^2 and thickness of 0.10 cm, was used as electrode. The weight of the electrode was around 1.9 and 3 mg. The gravimetric specific capacitance (C_s was determined from galvanostatic charge/discharge measurements in the voltage range of 0.0 to 1.0 V at different currents in the range of 1 to 50 mA.

Cyclic voltammograms were obtained at room temperature in the range of 0,0 to 0.9 V at different scan rates (1, 2, 5 e 10 mV s^{-1}). Electrochemical impedance spectroscopy (EIS) measurements were carried out in the frequency range from 10^{-4} to 10^{6} Hz with perturbation of sinusoidal amplitude of 15 mV (rms) and 10 points per frequency decade.

All electrochemical measurements were carried out at room temperature by a PGSTAT 302N Autolab potentiostat/galvanostat, for different aqueous solution electrolytes: 2 mol L^{-1} H_2SO_4, 1 mol L^{-1} Na_2SO_4 and 6 mol L^{-1} KOH.[4] In order to improve electrolyte infiltration, before the cell assembly, the electrodes were soaked in the electrolyte for 24 h.

3. Results and Discussion

3.1 Structure and morphology

The surface micrographs of ACF and Ag@ACF are illustrated in Figure 1a and 1b, respectively. Figure 1a shows the filament that constitutes the ACF has a fairly rough grave surface with the presence of sporicidal macro pores distributed throughout the filament surface. The silver deposited on ACF can be confirmed in Figure 1b and according to this image, the silver incorporation occurred throughout surface. In addition, the process resulted in the formation of non-uniformly distributed silver particles in nanometric scale. It is observed that in specific regions there is a formation of silver clusters on ACF surface. The estimated grain size formed on ACF surface is about of 200 nm diameter.

X-Ray diffractograms are shown in Figure 2. In both diffractograms diffraction peaks can be seen, located at 25.4º and 43.7º, which correspond to the carbon basal planes (002)

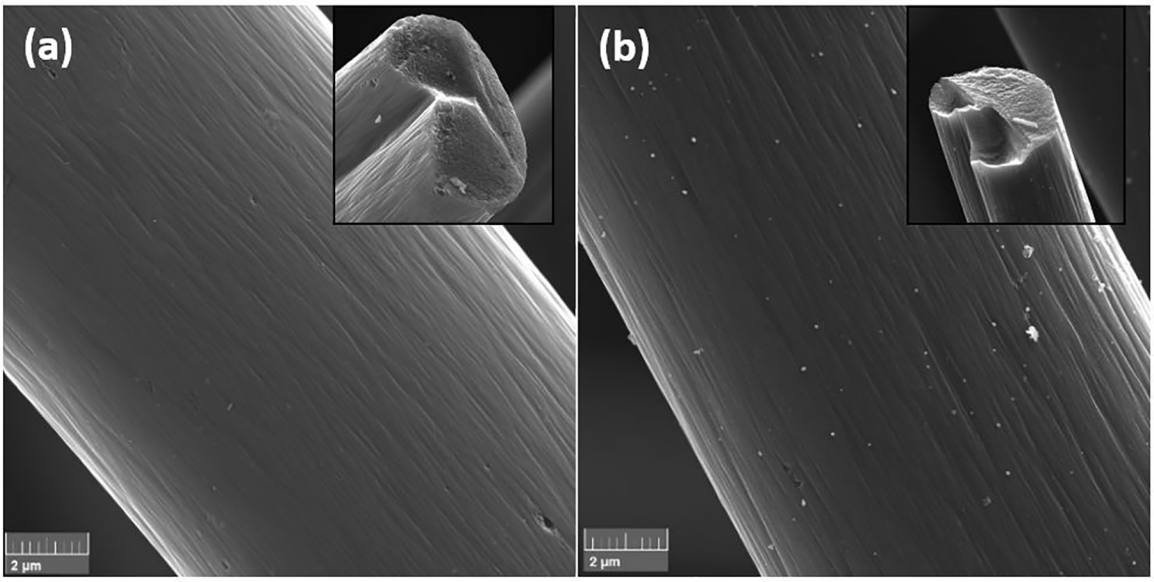

Figure 1. FEG-SEM images obtained for the samples at 20.000 of magnifications, and inset filament tip of (a) ACF and, (b) Ag@ACF.

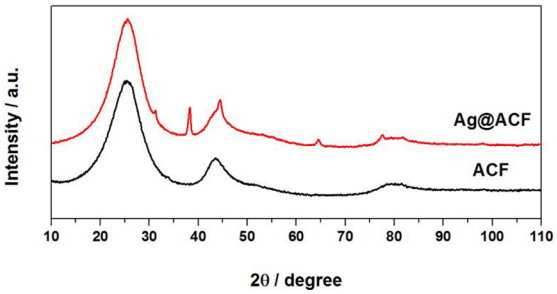

Figure 2. X-Ray diffractogram for ACF and Ag@ACF samples.

and (100).[27] In the Ag@ACF sample a metallic silver peaks can also identified at 38.3º, 44.5º, 64.5º and 77.5º, indexed as (111), (200), (220) and (311) crystal planes of the face-centered cubic (fcc) structure of metallic silver (reported data JCPDS 04-0783).[20]

The presence of silver particles on the Ag@ACF surface was also confirmed by XPS analysis. Detail spectrum of the Ag 3d emission line was deconvoluted into four fitted peaks, (Figure 3a). Those located at 368.1 and 374.1 eV correspond to metallic silver phase,[20] and those at 367.2 and 372.0 eV correspond to silver oxide phase.[28,29] This result demonstrates the coexistence of two different silver formations on the surface on the Ag@ACF. Taking into account that XPS resolution is limited to few nm deeper in the sample surface, these species exist on the surface of the analyzed material. On the other hand, if we consider XRD results, which provide information throughout the bulk of the material, only major peaks associated with metallic Ag are observed, while significant peaks associated to silver oxide formation is not distinguishable.

From the fit of O 1s emission line (Figure 3b), the peaks at 530.9 and 532.6 eV were assigned to AgO species[28] and C=O bond[30] respectively. Three peaks of the C 1s XPS spectrum are located at 284.7, 285.7 and 287.8 eV (Figure 3c), corresponding to the C-C, C-O and C=O bonds respectively.[30]

The XPS survey spectra analysis for ACF indicated the presence of two distinct chemical structures of oxygen and carbon. The high-resolution O 1s spectra (Figure 3d), in the range of (537-528 eV) reveal the presence of two peaks corresponding to C-OH and/or C-O-C groups and chemisorbed oxygen and/or water, indicating incorporation of oxygen functional groups on the carbon felt. The high-resolution C1s spectrum have each been resolved into four individual component peaks (Figure 3e) representing C-C, C=O, COO, O-C=O. The C 1s spectra clearly indicated a considerable degree of oxidation. From the point of view of the silver nanoparticles formation on the carbon fiber surface, the C-OH and/or C-O-C functional groups can act as the main active sites for the silver nanocrystals deposition.[21]. So, in the first step of the silver nanoparticle deposition onto the carbon fiber surface, the Ag^+ ions (from the $AgNO_3$ aqueous solution) are electrostatically adsorbed on the carbon fiber surface and are then reduced by the mentioned oxygenated functional groups.[21]

The adsorption/desorption isotherms curves of ACF and Ag@ACF samples are shown in Figure 4. The samples exhibit almost similar type-I adsorption/desorption isotherms, indicating typically microporous structures (pore diameter < 2 nm).[31] The porous structure parameters determined from the isotherms of the samples are presented in Table 1. These results demonstrate that the samples have similar

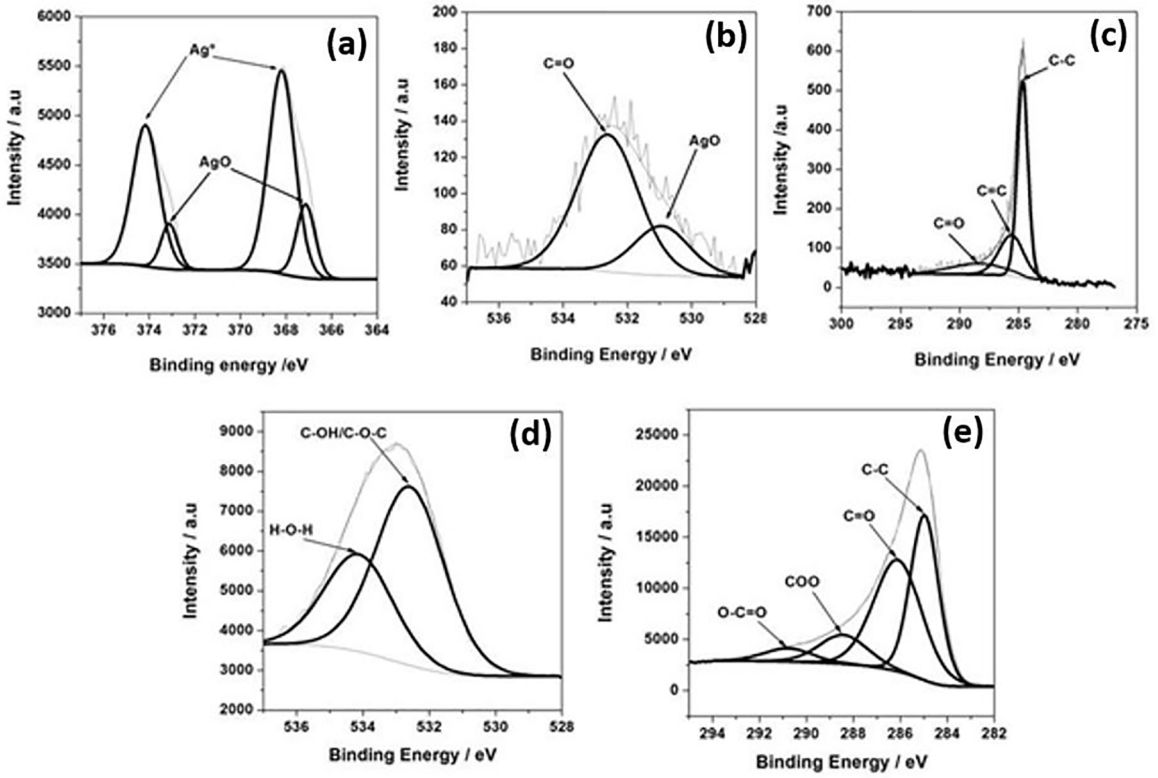

Figure 3. Deconvoluted XPS spectra of: (a) O 1s core level spectrum of Ag@ACF, (b) C 1s core level spectrum of Ag@ACF, and (c) Ag 3d core level spectrum, (d) O 1s core level spectrum of ACF, (e) C 1s core level spectrum of ACF.

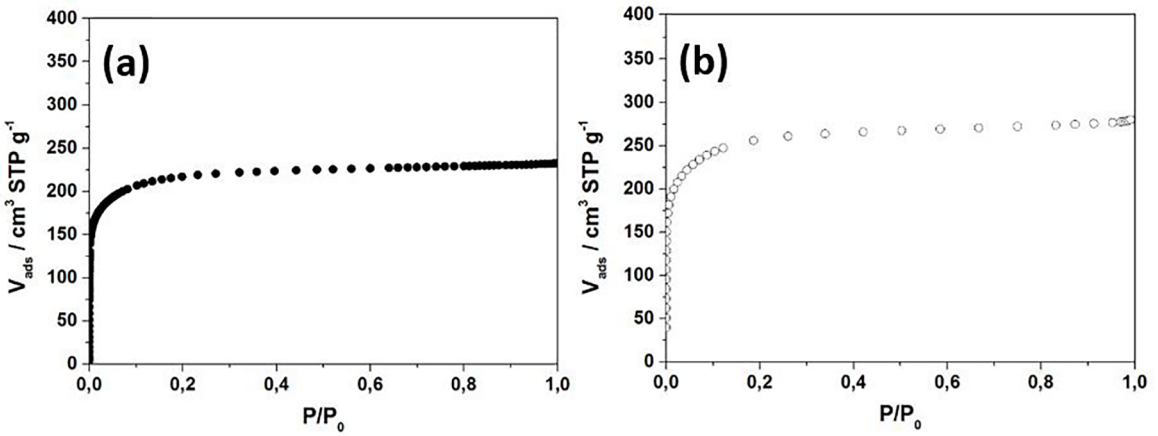

Figure 4. N_2 adsorption/desorption isotherms of (a) ACF sample and (b) Ag@ACF sample.

Table 1. Textural properties of the samples

Sample	W_o (cm^3g^{-1})	S_{mic} (m^2g^{-1})	L_o (nm)
ACF	0.30	590	1.0
Ag@ACF	0.36	606	1.2

W_o – micropore volume; S_{mic} – micropore area by Dubinin method ; L_o – modal micropore diameter

textural properties with similar W_o, S_{mic} of about 600 m^2g^{-1} and a L_o of about 1.0 nm. c that the chemical procedure used to incorporate silver particles on the fiber surface is "soft" having very little impact on the textural characteristics of the prepared fiber composite.

3.2 Electrochemical performance

The electric double layer and rapid redox reactions involved in electrochemical behavior of the ACF and Ag@ ACF electrodes were characterized by cyclic voltammetry analysis. These processes were evaluated by comparing the electrochemical behavior of the ACF and Ag@ACF electrodes, followed by a study involving the influence of the electrolyte

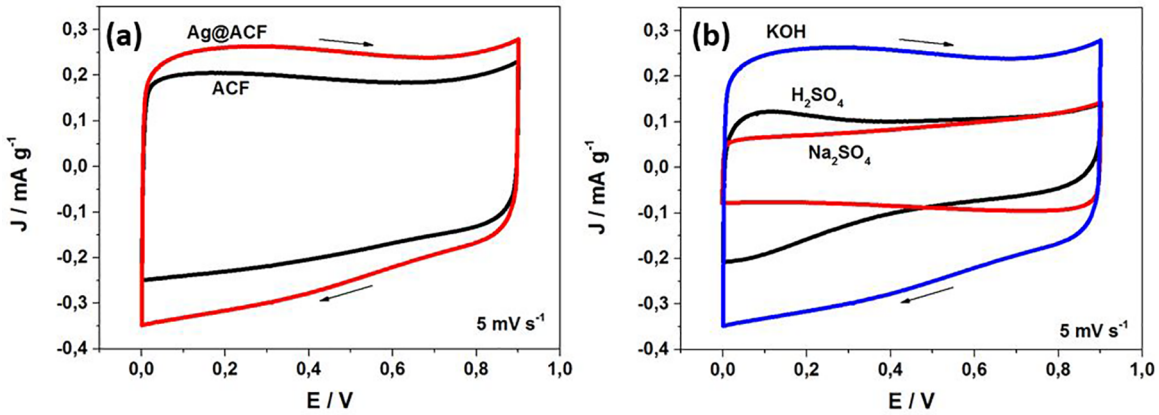

Figure 5. Cyclic voltammetry at 5mV s^{-1} scan rate on Ag@ACF at different aqueous electrolytes (a) show de difference between ACF and Ag@ACF in KOH medium, and (b) Ag@ACF performed at different aqueous electrolytes.

type. It is important to point out that the electrolyte type in a supercapacitor system is one of fundamental parameters to be defined for an effective operation.[4]

Figure 5(a) illustrates the cyclic voltammograms obtained for ACF and Ag@ACF electrodes using a 6 mol L^{-1} KOH aqueous solution. The result shows the significant contribution of the deposited silver nanoparticles.[30] There is an increase of the electric double layer capacitance in the voltammetric profile recorded at ACF and Ag@ACF electrodes. This result implies a fundamental role that silver nanoparticles play on the ACF electrode, by considerably increasing the exposed surface area available for the more effective occurrence of the electric layer double process. A non-symmetric profile regarding the charging/discharging of the electric double layer is also verified. According to the cyclic voltammograms characteristics, the ideal behavior of an electric double layer capacitor is expressed in the form of a symmetric rectangular shape.[24] The loss of this symmetry may be associated to possible reversible pseudo-faradaic reactions that occurred in a potential region at around 0.2 V. In addition, the resulting current profile becomes more inclined as the electric layer double discharging occurs, due to the difficulty the ions have to leave the interior of the ACF pores, probably caused by capillarity effect.

In addition to the KOH, H_2SO_4 and Na_2SO_4 electrolytes were also employed for evaluating the profile of the electric layer double capacitance. All these electrolytes have been commonly applied in supercapacitor systems.[4,32-34] In a more detailed analysis, it was possible to compare the formation of an electric double layer by using the three electrolytes. Figure 6b illustrates the cyclic voltammograms of the Ag@ACF electrode obtained in the three electrolytes at a scan rate of 5 mVs^{-1} in a potential range of 0.0V to 0.9V. As can be seen in Figure 5b, a considerable increase of the charging/discharging currents of the electric double layer can be verified in KOH solution when compared to H_2SO_4 and Na_2SO_4 solutions. One possible reason for this increase may be attributed to the high chemical affinity of the ACF to the OH^- ions sorbed on the electrode surface, due to its nucleophilic character. An enhancement on the charging/discharging current of about 2.5 times is verified in KOH solution.

Electrochemical impedance spectroscopy (EIS) was used to study the interface between the electrolyte and Ag@ACF. Figure 6 presents the Nyquist plot of measure impedance $Z(\omega)$ over a frequency range from 10^{-4} to 10^6 Hz at three different electrolytes. Nyquist plots are very similar and nearly vertical straight line are observed in each plot. The supercapacitors Nyquist plot may be divided in three different states, the resistance at high frequencies $Z'(\omega \rightarrow \infty)$, the capacitance at low frequencies and the ion penetration into ACF porous at the middle range frequency. The vertical line parallel to the imaginary part of the impedance, in the low frequency region, is associated with ideal capacitor behavior. This capacitive behavior may be linked to ion adsorption by the porosity of the ACF. In the middle range frequency there is the ion penetration into the porous ACF and at high frequencies, where the plots intercept the x-axis, the supercapacitor is associated with a resistance or combined resistances (intrinsic resistance of substrate, contact resistance and ionic resistance for electrolyte).[5]

The combined resistance is associated to the so-called equivalent series resistance of the cell (ESR) ($R_{ESR}=Z'(\omega \rightarrow \infty)$) .[35] In all the plots a partial semicircle is observed at middle range frequency. The electrolyte migration rate may influence the middle frequency range. The diameters of semicircles may be related with the faradaic resistance, which is associated with the mobility of ions between the electrode and electrolyte, limiting the diffusion of the involved species. The difference between the semicircles diameters may be associated to functional groups present in activated carbons. In the presence of three different electrolytes, the *ESR* decrease is more efficient in the KOH medium. According to the Nyquist plot, *ESR* increases in the order of solvents KOH < H_2SO_4 < Na_2SO_4. The transition between the kinetic and diffusion regimes, which is associated to a change from resistance to capacitance behavior at very low

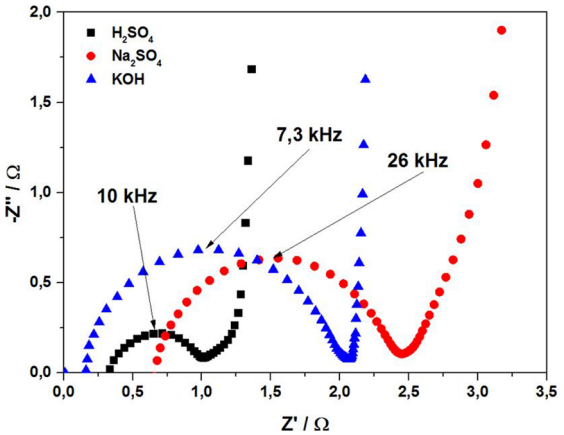

Figure 6. Nyquist plot corresponding to Ag@ACF performed at H_2SO_4, Na_2SO_4, and KOH.

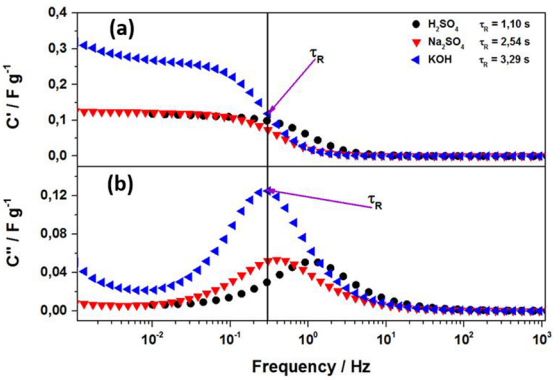

Figure 7. Progress of the a) real part and b) imaginary capacitance vs. frequency of Ag@ACF.

frequency, corresponds to knee, according to Lust et al[36] it is the so-called finite length effect. Besides, from the linear extrapolation of the Nyquist plot *Z″, Z′* to the condition *Z″=0*, the internal distribution resistance or pore resistance (R_{PORE}) may be estimated. The results show that the R_{PORE} increases in the order of solvents H_2SO_4 < KOH< Na_2SO_4. Several factors may influence the $R_{PORE,}$ such as specific conductivity, electrolyte resistance, ion radii and the migration of hydrated ions from inner pores.

In order to associate the supercapacitor frequency with the characteristic time constant $\tau_R=(2\pi f_R)^{-1}$, the capacitance can be calculated according to the following equation 1:

$$C(\omega)=\frac{-(Z''(\omega)+jZ')}{\omega|Z(\omega)|^2}=C'(\omega)+jC''(\omega) \qquad (1)$$

where $|Z(\omega)|$ is the impedance modulus. $C'(\omega)$ and $C''(\omega)$ are de real e imaginary parts of capacitance. The real part corresponds to deliverable capacitance, while the imaginary part is associated with the energy loss. The relaxation frequency f R can be estimated from maximum of *C″*. Figure 7 presents the evolution of $C'(\omega)$ and $C''(\omega)$ as a function of frequency. The maximum of $C''(\omega)$ is defined as the frontier between a pure capacitive and a pure resistive behavior. It can be observed that the relaxation frequencies obtained can be compared, which reveals the nature of the similarities in electrochemical properties between the systems. The relaxation times (τ_R) of 1.10s, 2.54s and 3.29s were obtained respectively for H_2SO_2, Na_2SO_4 and KOH. These results reveal that the supercapacitor is able to fully deliver its stored energy within a very short time. Although the difference in the relaxation time is not appreciable, it is important to remember some requirements associated to carbonaceous porous electrodes. According to Conway[24] the electrode must have enough volume to accommodate the electrolyte and also provide electrode pathways to access surface. This small difference in τ_R may be linked to the electrolyte penetration inside the porous and to the size of the porous electrode. Besides, when an AC-frequency is applied, the carbonaceous matrix responds in a different way, meaning that the transition between capacitive to resistive behavior shows some dependence with the choice of electrolyte. These results also demonstrate that the way the electrolyte accesses and interacts with the carbonaceous matrix influences the discharge power. In other words, there is a compromise between the capacity of stored energy, the time needed to deliver it and the choice of the electrolyte.

Galvanostatic charge-discharge (GCD) measurements were carried out to evaluate the rate performance of the composite materials. Figure 8a shows GCD curves at a current of 2 mA, in a potential window from 0 to 1 V, for the three electrolytes analyzed. GCD curves provide the main characteristics of supercapacitor behavior, which include specific capacitance (Eq. 2) and associated resistances.[3] The isosceles triangle shape point to a capacitive behavior and an excellent reversibility, this characteristic was confirmed by the behavior in cyclic voltammogram (Figure 5).[3,37] The linear stability of the potential over the time shows an absence of major faradaic processes,[38] indicating an excellent rate performance and a rapid ion transport mechanism.[39] Specific capacitance (C_s) was determined from discharge curves at each current using eqn (2):

$$C_S=2\frac{It_d}{E_2m_e} \qquad (2)$$

Where *I* is the current applied, t_d is the discharge time, E_2 is the voltage range during the discharge, and m_e is the mass of the electrode. This equation is used to a two electrode symmetrical cell, and the reason for multiplying the equation by 2 is that the capacitance of the two electrodes is considered.[40]

Long term cycling performance is another parameter for estimating the stability of ES. Continuous charge/discharge cycles were carried out over 3000 cycles at a current of 10 mA, as shown in Figure 8b. The capacitance retention was constant for the three electrolytes, about 98%, which means that the cell loses about 2% of this initial capacitance after

3000 cycles in relation to the capacitance in the first cycle. This constancy may be associated with the non-modification of the pore accessibility by electrochemical redox reactions.[38]

The Ragone plot is shown in Figure 9a. The gravimetric energy density W_S was calculated according to: $W_S=(1/2)C_S.V^2$ where C_S is the specific capacitance measured at each current density and Vis the voltage range during the galvanostatic discharge at each current density. The gravimetric power density P_S was calculated as: $P_S=W_S/t_d$ where t_d is the discharge time. In the Ragone plot the maximum energy density was 23 Wh kg^{-1} (with a power density of 383 W kg^{-1}) for Ag@FCA in alkaline medium and the maximum power density was 24 kW kg^{-1} (with an energy density of 10 Wh kg^{-1}) for ACF in neutral medium. These values are higher than other devices reported previously.[5,9,33,39] The dependence of the gravimetric specific capacitance (C_s) as function of the current density is shown in Figure 9b. It can be seen that the Ag@ACF sample has higher C_s both low and high currents densities with KOH electrolyte. At low current (1 mA), the Cs value of the Ag@ACF sample is 169 F g^{-1} while the corresponding value for the ACF sample is 113 F g^{-1} (not show in Figure 9b), both in KOH electrolyte. All the samples present an excellent rate capability, which can be mainly ascribed to reliable electrical connections between the Ag nanoparticles and the activated carbon fiber structure.

4. Conclusions

A novel type of activated carbon felts decorated with silver nanoparticles composites were investigated as electrode material for electrochemical capacitors in different aqueous electrolytes. The process of silver deposition was very simple, cheap and safe. Such a process gives a deposition of metallic silver particles in nano size dimension, which probably increased its surface area. This unique architecture of highly porous materials provides a facile, scalable, and low-cost opportunity for fabricating energy storage devices. Despite the low quantity of silver deposited there was a significant increase in the capacitance of the composite. The type of electrolyte used also has a significant influence on the

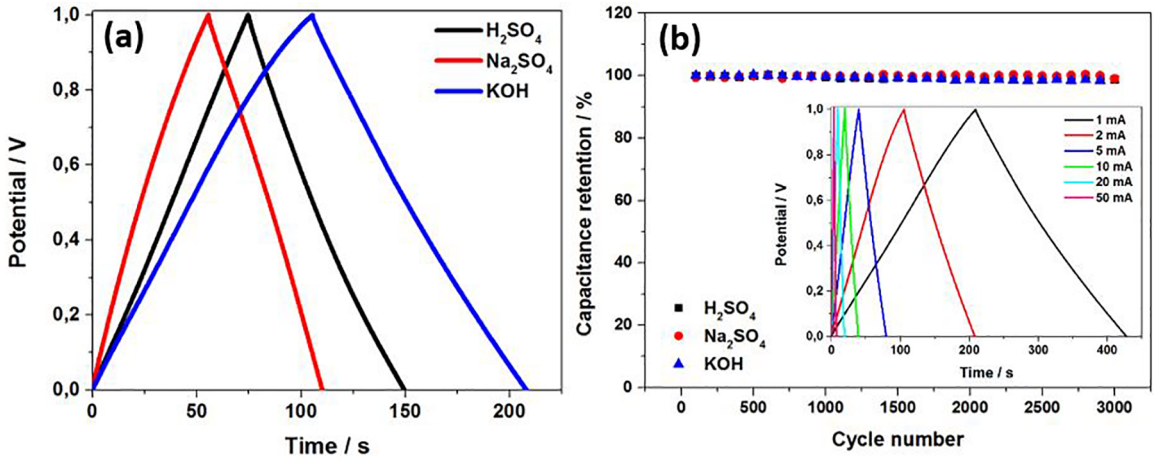

Figure 8. a) charge/discharge curves at current of 2 mA of Ag@ACF, and b) progress of capacitance retention over charge/discharge cycles with a current of 10 mA of Ag@ACF, inset: charge/discharge curves at several currents of Ag@ACF in KOH.

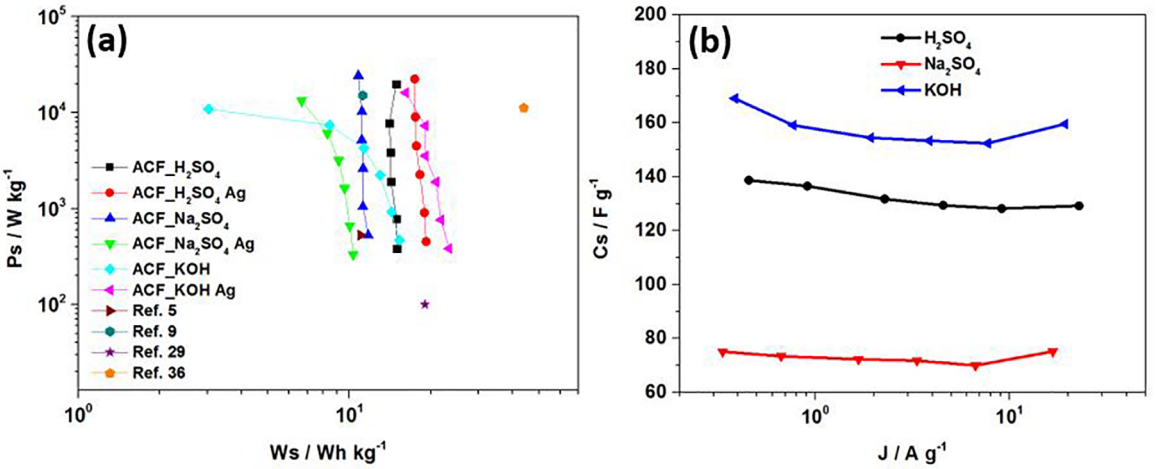

Figure 9. a) Gravimetric power density vs. gravimetric energy density of ACF and Ag@FCA at different electrolytes compared with data in other literature, and b) specific capacity vs. current density of Ag@ACF.

capacitance of the devices. The characteristic electrochemical impedance for this material showed relaxation times constant of 1,10s, 2,54s, and 3,29s for H_2SO_4, Na_2SO_4, and KOH, respectively, which are very good relaxation times for high-performance supercapacitor devices. A high voltage window of 1.0 V was observed for a symmetric Ag@carbon/Ag@ carbon electrodes cell offering good rate capability with a reasonable specific capacitance of 169 Fg^{-1} (KOH), 138 Fg^{-1} (H_2SO_4), and 77 Fg^{-1} (Na_2SO_4), energy density of 23 $Whkg^{-1}$ (KOH), 19 $Whkg^{-1}$ (H_2SO_4), and 10 $WHkg^{-1}$ (Na_2SO_4) and excellent cyclability. These results in alkaline 6 M KOH electrolyte are quite interesting, encouraging and showed the applicability of Ag@ACF demonstrating the exciting potential for a low-cost porous carbon, which could attract interest from the industry for potential application in energy storage.

5. Acknowledgments

The author would like to thank PCI-MCTI (Institutional Process Number 454779/2015-1 and Individual Process Number 170136/2016-7) and Capes for financial support, ITA and INPE for the support and infrastructure.

6. References

1. Béguin F, Frackowiak E. *Supercapacitors: Materials, Systems, and Applications*. Weinheim: Wiley-VCH Verlag; 2013.
2. Ke Q, Wang J. Graphene-based materials for supercapacitor electrodes - A review. *Journal of Materiomics*. 2016;2(1):37-54.
3. González A, Goikolea E, Barrena JA, Mysyk R. Review on supercapacitors: Technologies and materials. *Renewable and Sustainable Energy Reviews*. 2016;58:1189-1206.
4. Zhong C, Deng Y, Hu W, Qiao J, Zhang L, Zhang J. A review of electrolyte materials and compositions for electrochemical supercapacitors. *Chemical Society Reviews*. 2015;44(21):7484-7539.
5. Wen Y, Qin T, Wang Z, Jiang X, Peng S, Zhang J, et al. Self-supported binder-free carbon fibers/MnO_2 electrodes derived from disposable bamboo chopsticks for high-performance supercapacitors. *Journal of Alloys and Compounds*. 2017;699:126-135.
6. Noh J, Yoon CM, Kim YK, Jang J. High performance asymmetric supercapacitor twisted from carbon fiber/MnO_2 and carbon fiber/MoO_3. *Carbon*. 2017;116:470-478.
7. Ma X, Du X, Li X, Hao X, Jagadale AD, Abudula A, et al. In situ unipolar pulse electrodeposition of nickel hexacyanoferrate nanocubes on flexible carbon fibers for supercapacitor working in neutral electrolyte. *Journal of Alloys and Compounds*. 2017;695:294-301.
8. Cakici MM, Kakarla RR, Alonso-Marroquin F. Advanced electrochemical energy storage supercapacitors based on the flexible carbon fiber fabric-coated with uniform coral-like MnO_2 structured electrodes. *Chemical Engineering Journal*. 2017;309:151-158.
9. He T, Su Q, Yildiz Z, Cai K, Wang Y. Ultrafine Carbon Fibers with Hollow-Porous Multilayered Structure for Supercapacitors. *Electrochemica Acta*. 2016;222:1120-1127.
10. Shang X, Chi JQ, Lu SS, Gou JX, Dong B, Li X, et al. Carbon fiber cloth supported interwoven WS2 nanosplates with highly enhanced performances for supercapacitors. *Applied Surface Science*. 2017;392:708-714.
11. Ye Z, Li T, Ma G, Peng X, Zhao J. Morphology controlled MnO2 electrodeposited on carbon fiber paper for high-performance supercapacitors. *Journal of Power Sources*. 2017;351:51-57.
12. Han S, Lin L, Zhang K, Luo L, Peng X, Hu N. ZnWO4 nanoflakes decorated NiCo2O4 nanoneedle arrays grown on carbon cloth as supercapacitor electrodes. *Materials Letters*. 2017;193:89-92.
13. Wang K, Yan R, Zhao N, Tian X, Li X, Lei S, et al. Bio-inspired hollow activated carbon microtubes derived from willow catkins for supercapacitors with high volumetric performance. *Materials Letters*. 2016;174:249-252.
14. Karnan M, Subramani K, Srividhya PK, Sathish M. Electrochemical Studies on Corncob Derived Activated Porous Carbon for Supercapacitors Application in Aqueous and Non-aqueous Electrolytes. *Electrochimica Acta*. 2017;228:586-596.
15. Teo EYL, Muniandy L, Ng EP, Adam F, Mohamed AR, Jose R, et al. High surface area activated carbon from rice husk as a high performance supercapacitor electrode. *Electrochimica Acta*. 2016;192:110-119.
16. Yuan W, Han G, Chang Y, Li M, Xiao Y, Zhou H, et al. Performance of flexible capacitors based on polypyrrole/carbon fiber electrochemically prepared from various phosphate electrolytes. *Applied Surface Science*. 2016;387:902-911.
17. Patil DS, Pawar SA, Devan RS, Mali SS, Gang MG, Ma YR, et al. Polyaniline based electrodes for electrochemical supercapacitor: Synergistic effect of silver, activated carbon and polyaniline. *Journal of Electroanalytical Chemistry*. 2014;724:21-28.
18. Usman M, Pan L, Sohail A, Mahmood Z, Cui R. Fabrication of 3D vertically aligned silver nanoplates on nickel foam-graphene substrate by a novel electrodeposition with sonication for efficient supercapacitors. *Chemical Engineering Journal*. 2017;311:359-366.
19. Kalambate PK, Dar RA, Karna SP, Srivastava AK. High performance supercapacitor based on graphene-silver nanoparticles-polypyrrole nanocomposite coated on glassy carbon electrode. *Journal of Power Sources*. 2015;276:262-270.
20. Yuan L, Wan C, Ye X, Wu F. Facial Synthesis of Silver-incorporated Conductive Polypyrrole Submicron Spheres for Supercapacitors. *Electrochimica Acta*. 2016;213:115-123.
21. Vanitha M, Keerthi, Cao P, Balasubramanian N. Ag nanocrystals anchored CeO_2/graphene nanocomposite for enhanced supercapacitor applications. *Journal of Alloys and Compounds*. 2015;644:534-544.
22. Huang J, Wu H, Cao D, Wang G. Influence of Ag doped CuO nanosheet arrays on electrochemical behaviors for supercapacitors. *Electrochimica Acta*. 2012;75:208-212.

23. Kim KS, Park SJ. Bridge effect of silver nanoparticles on electrochemical performance of graphite nanofiber/polyaniline for supercapacitor. *Synthetic Metals*. 2012;162(23):2107-2111.

24. Conway BE. *Electrochemical Supercapacitors: Scientific Fundamentals and Technological Applications*. New York: Springer US; 1999.

25. Marcozzu SJ, Cuña A, Tancredi N, Mendez E, Bernardi HH. Microporous activated carbon fiber felt from Brazilian textile PAN fiber: preparation, characterization and application as super capacitor electrode. *Revista Brasileira de Aplicações no Vácuo*. 2016;35:58.

26. Stoeckli F, Centeno TA. Optimization of the characterization of porous carbons for supercapacitors. *Journal of Materials Chemistry A*. 2013;1(23):6865-6873.

27. Li ZQ, Lu CJ, Xia ZP, Zhou Y, Luo Z. X-ray diffraction patterns of graphite and turbostratic carbon. *Carbon*. 2007;45(8):1686-1695.

28. Hashim M, Hua C, Wang X, Wan B, Xu J. Room temperature synthesis and photocatalytic property of AgO/Ag2Mo2O7 heterojunction nanowires. *Materials Research Bulletin*. 2012;47(11):3383-3389.

29. Heine C, Eren B, Lechner BAJ, Salmeron M. A study of the O/Ag(111) system with scanning tunneling microscopy and X-ray photoelectron spectroscopy at ambient pressures. *Surface Science*. 2016;652:51-57.

30. Zhou JH, Sui ZJ, Zhu J, Li P, Chen D, Dai YC, et al. Characterization of surface oxygen complexes on carbon nanofibers by TPD, XPS and FT-IR. *Carbon*. 2007;45(4):785-796.

31. Marsh H, Rodríguez-Reinoso F. *Activated Carbon*. Oxford: Elsevier; 2006. 554 p.

32. Frackowiak E, Abbas Q, Béguin F. Carbon/carbon supercapacitores. *Journal of Energy Chemistry*. 2013;22(2):226-240.

33. Bello A, Manyala N, Barzegar F, Khaleed AA, Momodu DY, Dangbegnon JK. Renewable pine cone biomass derived carbon materials for supercapacitor application. *RSC Advances.* 2016;6(3):1800-1809.

34. Zhang LL, Zhao XS. Carbon-based materials as supercapacitor electrodes. *Chemical Society Reviews*. 2009;38(9):2520-2531.

35. Choi BG, Hong J, Hong WH, Hammond PT, Park H. Facilitated Ion Transport in All-Solid-State Flexible Supercapacitors. *ACS Nano*. 2011;5(9):7205-7213.

36. Lust E, Jänes A, Arulepp M. Influence of solvent nature on the electrochemical parameters of electrical double layer capacitors. *Journal of Electroanalytical Chemistry*. 2004;562(1):33-42.

37. Zhang L, Jiang Y, Wang L, Zhang C, Liu S. Hierarchical porous carbon nanofibers as binder-free electrode for high-performance supercapacitor. *Electrochimica Acta*. 2016;196:189-196.

38. Taberna PL, Simon P, Fauvarque JF. Electrochemical Characteristics and Impedance Spectroscopy Studies of Carbon-Carbon Supercapacitors. *Journal of The Electrochemical Society*. 2003;150(3):A292-A300.

39. Choi BG, Yang M, Hong WH, Choi JW, Huh YS. 3D Macroporous Graphene Frameworks for Supercapacitors with High Energy and Power Densities. *ACS Nano*. 2012;6(5):4020-4028.

40. Abdulhakeem B, Farshad B, Damilola M, Fatemeh T, Mopeli F, Julien D, et al. Morphological characterization and impedance spectroscopy study of porous 3D carbons based on graphene foam-PVA/phenol-formaldehyde resin composite as an electrode material for supercapacitors. *RSC Advances*. 2014;4(73):39066-39072.